J. Biochem. **139**, 789–795 (2006)
doi:10.1093/jb/mvj088

Three-Dimensional Structure of Rat-Liver Acyl-CoA Oxidase in Complex with a Fatty Acid: Insights into Substrate-Recognition and Reactivity toward Molecular Oxygen

Keiji Tokuoka[1], Yoshitaka Nakajima[1,*], Ken Hirotsu[1], Ikuko Miyahara[1], Yasuzo Nishina[2], Kiyoshi Shiga[2], Haruhiko Tamaoki[3], Chiaki Setoyama[3], Hiromasa Tojo[4] and Retsu Miura[3,†]

[1]Department of Chemistry, Graduate School of Science, Osaka City University, Sugimoto, Sumiyoshi-ku, Osaka 558-8585; Departments of [2]Molecular Physiology and [3]Molecular Enzymology, Graduate School of Medical Sciences, Kumamoto University, Honjo, Kumamoto 860-8556; and [4]Department of Biochemistry and Molecular Biology, Graduate School of Medicine, Osaka University, Yamadaoka, Suita 565-0871

Received February 5, 2006; accepted March 1, 2006

The three-dimensional structure of rat-liver acyl-CoA oxidase-II (ACO-II) in a complex with a C12-fatty acid was solved by the molecular replacement method based on the uncomplexed ACO-II structure. The crystalline form of the complex was obtained by cocrystallization of ACO-II with dodecanoyl-CoA. The crystalline complex possessed, in the active-site crevice, only the fatty acid moiety that had been formed through hydrolysis of the thioester bond. The overall dimeric structure and the folding pattern of each subunit are essentially superimposable on those of uncomplexed ACO-II. The active site including the flavin ring of FAD, the crevice embracing the fatty acyl moiety, and adjacent amino acid side chains are superimposably conserved with the exception of Glu421, whose carboxylate group is tilted away to accommodate the fatty acid. One of the carboxyl oxygens of the bound fatty acid is hydrogen-bonded to the amide hydrogen of Glu421, the presumed catalytic base, and to the ribityl 2′-hydroxyl group of FAD. This hydrogen-bonding network correlates well with the substrate recognition/activation in acyl-CoA dehydrogenase. The binding mode of C12-fatty acid suggests that the active site does not close upon substrate binding, but remains spacious during the entire catalytic process, the oxygen accessibility in the oxidative half-reaction thereby being maintained.

Key words: acyl-CoA oxidase, complex with a fatty acid, reactivity with oxygen, substrate recognition, three-dimensional structure.

Abbreviations: ACD, acyl-CoA dehydrogenase; ACO, acyl-CoA oxidase; MCAD, medium-chain acyl-CoA dehydrogenase

The fatty acid degradation through β-oxidation in mammals is known to proceed in two different cellular compartments, mitochondria and peroxisomes (see Ref. *1* for a historical overview). The former contain the pathway initiated by acyl-CoA dehydrogenases (ACDs) while the latter foster that initiated by acyl-CoA oxidases (ACOs). An ACO [EC 1.3.3.6] is a flavooxidase with one non-covalently bound FAD per subunit as the prosthetic group and catalyzes dehydrogenation of acyl-CoA yielding *trans*-2-enoyl-CoA in the reductive half-reaction (Scheme 1). ACOs and ACDs belong to the same superfamily (*2*) and cause the same catalytic dehydrogenation of acyl-CoA to the corresponding *trans*-2-enoyl-CoA in the reductive half-reaction. In contrast, they differ completely in the oxidative half-reaction; ACO utilizes molecular oxygen to reoxidize reduced flavin produced in the reductive half-reaction while ACD passes electrons to electron-transferring flavoprotein to regenerate an oxidized flavin (see a recent review Ref. *3* and references cited therein). We have cloned two different isoforms of rat-liver ACO (ACO-I and ACO-II), and separately expressed, purified and characterized them (*4*). We then solved the crystal structure of ACO-II, the first three-dimensional structure of ACO ever solved, and revealed the structural basis for its reactivity toward acyl-CoA as well as toward molecular oxygen (*5*). The three-dimensional structure of a plant ACO was reported very recently and it was shown that its structural features in terms of overall folding as well as active-site architecture closely resemble those of rat ACO-II (*6*).

Although it has been known for quite some time that ACOs and ACDs belong to the same superfamily (*2*) and cause the identical reductive half-reaction, *i.e.*, α-β dehydrogenation of acyl-CoA, the investigation of ACOs on the molecular level has been relatively limited as compared to that of ACDs due primarily to the lack of three-dimensional structures. Moreover, the mechanistic studies (see Ref. *7* for a recent review) on ACDs have mainly been focused on their reductive half-reactions and not much on their oxidative half-reactions. However, the oxidative half-reactions of the ACO-ACD superfamily, particularly

*Present address: Graduate School of Biomedical Sciences, Nagasaki University, 1-14 Bunkyo-machi, Nagasaki 852-8521.

†To whom correspondence should be addressed. Fax: +81-96-373-5066, E-mail: miura@gpo.kumamoto-u.ac.jp

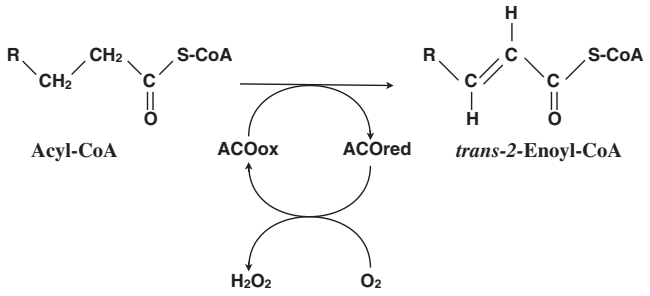

Scheme 1. **Reaction catalyzed by acyl-CoA oxidase (ACO).** ACOox and ACOred stand for the oxidized and reduced forms of ACO, respectively.

their reactivity toward molecular oxygen, are of fundamental importance as to the mechanism of flavoenzymes on the one hand, and as to the physiological roles of ACO and ACD on the other hand. From a mechanistic point of view, we have postulated that the reactivity of reduced flavin toward oxygen is controlled through modulation of the resonance hybridization of an anionic reduced flavin so as to fine-tune the nucleophilicity or electron density of C(4*a*) of the anionic reduced flavin (*8*). Meanwhile, the reactivity of reduced flavin should be properly controlled in order for a flavoenzyme to play its physiological role; the reaction of ACD with oxygen is strictly suppressed so that electrons from reduced flavin are passed on to the respiratory chain for ATP synthesis. The ATP synthesis would be irrelevantly bypassed were it not for the strict suppression of reaction with oxygen. Thus, the ACO-ACD pair will turn out to be an excellent combination of proteins for studying the mechanism underlying the reaction of the reduced form with molecular oxygen in view of their identical reductive half-reactions but totally different oxidative half-reactions. Both rat ACO-II (*5*) and plant ACO (*6*) are characterized by a spacious active-site pocket and the solvent accessibility favorable for oxygen approach in the oxidative half-reaction. However, these active-site structures have only been demonstrated for the uncomplexed resting state and it remains unknown whether they remain open to oxygen approach when the substrate or product is bound within them. In order to solve these issues we attempted in this study to solve the three-dimensional structure of rat ACO-II in a complex form with a substrate or product. The structure is expected to offer valuable information with respect to substrate recognition/activation in the reductive half-reaction as well as to the reactivity toward molecular oxygen in the oxidative half-reaction.

MATERIALS AND METHODS

Materials—Rat liver ACO-II was expressed in the *Escherichia coli* expression system and purified according to the previously reported procedure (*4*). Dodecanoyl-CoA (lauroyl-CoA) was a product of Sigma and the other chemicals used in this study were from commercial sources and of the highest grade available.

Cocrystallization of ACO-II in the Presence of Dodecanoyl-CoA and Data Collection—The initial crystallization conditions were optimized using Wizard I and II crystal screens (Emerald Biostructures) with 19.0 mg/ml protein and a 100-molar excess of dodecanoyl-CoA in 10 mM Tris-HCl (pH 7.5). Crystals were grown at 293 K by the hanging-drop vapor-diffusion method under oil (*9*). The optimized crystallization conditions involved mixing 2 μl of the protein-ligand mixture with an equivalent volume of a reservoir solution comprising 20% polyethyleneglycol 8000, 2.0 M NaCl and 0.1 M HEPES (pH 7.5). The yellow crystals thus obtained belong to the space group $C222_1$ with one monomer per asymmetric unit, and approximately 48% of the crystal volume is occupied by solvent (*10*). The unliganded enzyme has been reported to be crystallized with the space group $P2_12_12_1$ with one dimer per asymmetric unit (*5*).

Table 1. **Data collection and refinement statistics.**

Data collection	
space group	$C222_1$
lattice parameter (Å)	
a	85.5
b	103.2
c	161.9
temperature (K)	100
wavelength (Å)	1.00
resolution range (Å)	20.0–2.07
no. of reflections	
observation	241,820
unique	43,475 (4,081)[a]
completeness (%)	96.9 (93.6)
R_{merge} *b* (%)	7.6 (28.2)
Refinement	
resolution limit (Å)	41.7–2.07
R_{factor} (%)	19.9 (20.5)
R_{free} (%)	24.1 (25.7)
deviations	
bond lengths (Å)	0.006
bond angles (deg)	1.2
Mean B factors	
main chain atoms (Å^2)	19.8
side chain atoms (Å^2)	22.4
hetero atoms (Å^2)	29.2
waters molecules (Å^2)	28.0

[a]The values in parentheses are for the highest resolution shells. [b]$R_{merge} = \Sigma_{hkl}\Sigma_i|I_{hkl,i} - \langle I_{hkl}\rangle| / \Sigma_{hkl}\Sigma_i I_{hkl,i}$, where I = observed intensity and $\langle I\rangle$ = average intensity for multiple measurements.

The X-ray diffraction data set was collected to 2.07-Å resolution at 100 K using the wavelength of 1.00 Å on NW-12A stations equipped with an ADSC Quantum 4R CCD detector system at the Photon Factory, KEK (Tsukuba, Japan). A cryoprotectant solution of 13% glycerol in the reservoir buffer was used for flash-freezing of the crystals in liquid nitrogen. The data set was processed and scaled using program HKL2000 (*11*) (Table 1).

Structure Determination and Refinement—The structure of the ACO-II complex was determined with program AmoRe (*12*), using the previously determined structure of the unliganded ACO-II (*5*, PDB ID: 1IS2) monomer as a search model. The modeling of the polypeptide chain was performed using program O (*13*). The structure was refined by simulated annealing and energy minimization with program CNS (*14*). When the R_{factor} value decreased to below 30%, the difference Fourier map around the active site exhibited a residual electron density corresponding to

the acyl moiety of dodecanoyl-CoA, but no clear electron density for the CoA moiety was observed. As the result of ligand extraction and mass-spectroscopic analysis, 3-hydroxydodecanoate, the major component of the bound fatty acid, was assigned to the peak in a simulated annealing 2*F*o – *F*c map. Water molecules were picked up from the 2*F*o – *F*c map on the basis of the peak height (1.0 σ) and distance criteria (4.0 Å from protein and solvent). The water molecules with thermal factors above 40 $Å^3$ were removed from the list. Further model building and refinement cycles resulted in an R_{factor} of 20.1% and an R_{free} of 24.3%, calculated for 42,480 reflections (Table 1). During the last step of the refinement, unambiguous water molecules were added including those with temperature factors higher than 40 $Å^3$. The occupancy factor of 3-hydroxydodenanoate was determined to be 0.87. The model lacks 32 residues (270–280, 355–364, 459–474) due to uninterpretable electron density. The lack of two loop regions (270–280, 459–474) is also shared by unliganded ACO-II (*5*). Alanine models were applied to 6 residues (113, 114, 352, 353, 354, 365), because no interpretable electron density was observed for their side chains. The model was of good quality with almost all the residues falling in the most favorable (93.5%) and allowed regions (6.1%) of the Ramachandran plot, when the stereochemistry was assessed with PROCHECK (*15*). Trp176 was assigned in the disallowed region, as it was for the unliganded enzyme (*5*). This may be related with the orientation of the side chain; the indole ring of Trp176 is in a stacking orientation as to the flavin ring, covering the *si*-face of flavin, while the *re*-face is occupied by the fatty acid (see "RESULTS AND DISCUSSION").

Extraction of Fatty Acids from the Crystal Preparation and Mass Spectroscopic Analysis—After crystals had been allowed to grow in the cocrystallization mixture, the preparation mixture was diluted 24 times with 0.4 N HCl containing 1% KCl to decrease the protein concentration and viscosity. Fatty acids were extracted into the upper phase by the two-phase partition method of Dole and Meinertz (*16*). The upper phase was transferred to a new glass tube and then evaporated under a nitrogen gas flow. The extracted fatty acids were dissolved in methanol containing 10 mM ammonium formate, and then directly infused into the electrospray ionization (ESI) source in a Mariner ESI/time-of-flight mass spectrometer at the flow rate of 5 μl/min. An ESI voltage of 3 kV and a nozzle potential of 80 V were applied.

RESULTS AND DISCUSSION

Structure of ACO-II in a Complex with a Ligand—We attempted to obtain the crystalline form of the ACO-II-ligand complex by soaking substrates and substrate analogs in crystalline ACO-II. However, all the soaking experiments were unsuccessful due to cracks developing in the crystals. We subsequently cocrystallized ACO-II in the presence of substrate dodecanoyl-CoA (lauroyl-CoA) and obtained crystals of ACO-II with a bound ligand. The overall dimeric structure of cocrystallized ACO-II is shown in Fig. 1. As will be shown later, the ligand bound in the active site is drawn as 3-hydroxydodecanoate, the predominant component of the bound ligand. The two subunits are correlated with each other through a crystallographic two-fold axis. The overall folding pattern of the dimeric complex is practically superimposable on that of uncomplexed ACO-II (*5*). This is better envisaged when the equivalenced Cα atoms of the subunit structures of complexed ACO-II are superposed on those of uncomplexed ACO-II (Fig. 2). These observations suggest strongly that the protein conformation does not change upon ligand binding, which is contrary to our previous expectation that the active site might close when the substrate binds to it (*5*). Namely, the active site remains spacious irrespective of whether the enzyme is in the resting state with a vacant active site or in the acting state with a substrate or product bound in the active site and, therefore, oxygen can freely gain access to the reduced form of flavin during the oxidative half-reaction.

Active Site and Ligand-Binding Mode—Figure 3 shows superpositioning of the active sites for the uncomplexed and complexed states, the latter embracing the fatty acid moiety derived from the substrate dodecanoyl-CoA. As will be shown in the subsequent section, the fatty acid species extracted from the cocrystallization preparation is a mixture of dodecenoate and hydroxydodecanoate, the latter predominating over the former. Though the electron density for the ligand should reflect the weighted average of the two components, the electron density in Fig. 4 is fitted to the predominant component, 3-hydroxydodecanoate (see the subsequent section for structural assignment of the ligand). It is noteworthy that only electron density for the fatty acid moiety on the *re*-face of the flavin ring, *i.e.*, none corresponding to the CoA segment, was observed in the substrate-binding pocket. Although not shown in Fig. 4, the indole ring of

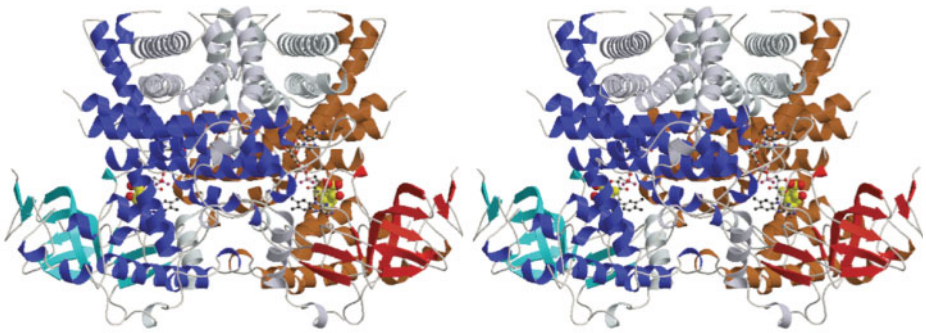

Fig. 1. **Stereoview of the overall dimeric structure of ACO-II cocrystallized with dodecanoyl-CoA.** Note that the bound ligand is 3-hydroxydodecanoate drawn as a CPK model. The coenzyme FAD is drawn as a ball-and-stick model.

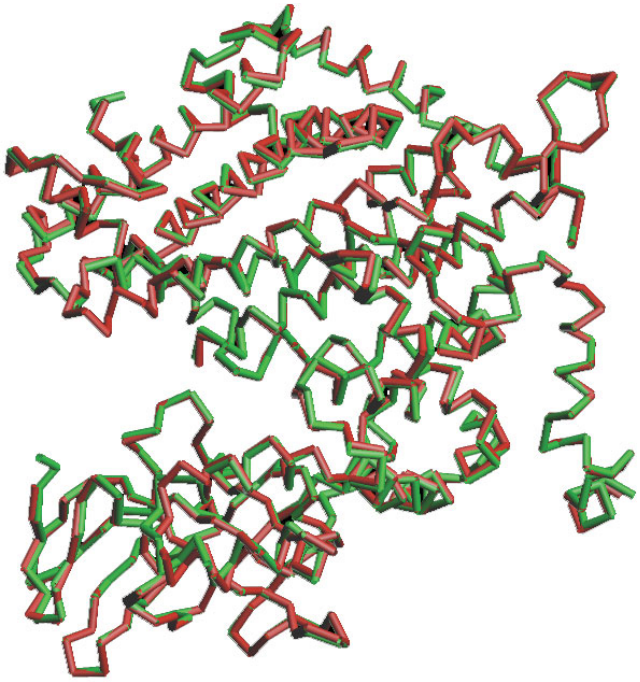

Fig. 2. **Superpositioning of Cα-tracings of complexed (green) and uncomplexed (red) ACO-II.**

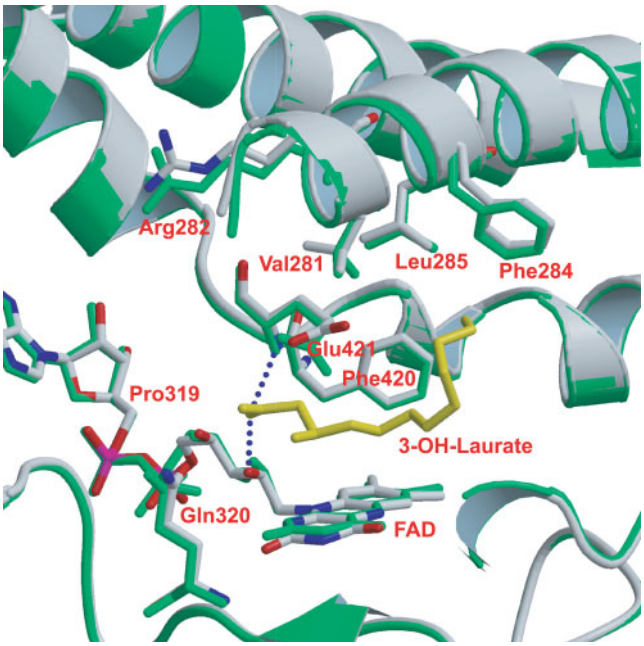

Fig. 3. **Superpositioning of the active-site structures of complexed (grey with oxygen and nitrogen in red and blue, respectively) and uncomplexed (green) ACO-II.** 3-Hydroxydodecanoate is drawn in yellow. Blue dotted lines represent the hydrogen bonding network between the carboxyl oxygen of the bound fatty acid with the backbone amide group of Glu421 and the ribityl-2′-hydroxyl group of FAD.

Trp176 covers the *si*-face, as it does in the unliganded structure (*5*). The hydrocarbon chain of the fatty acid extends along the acyl chain-binding crevice and its length matches that of the C-12 fatty acid included in the substrate dodecanoyl-CoA that was cocrystallized with ACO-II. The side chain of Glu421, the postulated catalytic base that abstracts the α-proton of acyl-CoA (*5*), has changed its orientation in the complexed state, pointing away from the flavin ring to accommodate the fatty acyl moiety. Note the proximity, the interatomic distance being 3.1 Å, of the α-carbon of the bound fatty acid and one of the carboxyl oxygens of Glu421 (dotted line in Figs. 4 and 5), the presumed catalytic base for abstraction of the α-proton of substrate. The mutual alignment of the fatty acid, Glu421 carboxylate and FAD, with the interatomic distances, is illustrated in Fig. 5. The positioning of the carboxyl oxygen relative to the fatty acid α-position is indicative that the Glu421 carboxylate is the catalytic base for abstraction of the substrate α-proton, which is activated by the hydrogen-bonding network at the thioester carbonyl, as discussed below (Scheme 2).

One of the carboxyl oxygens of the C-12 fatty acid is hydrogen-bonded to the ribityl-2′-hydroxyl group of FAD and to the backbone amide hydrogen of Glu421, the catalytic base (Fig. 3, dotted lines, and Fig. 5, thick dashed lines). The interatomic distances corresponding to these hydrogen bonds are 2.5 and 2.9 Å, respectively. This hydrogen-bonding network is reminiscent of that for the recognition and activation of substrate acyl-CoA in medium-chain acyl-CoA dehydrogenase (MCAD) (*17*), the most extensively investigated member of the ACD family; the carbonyl oxygen of the substrate thioester forms a hydrogen bond with the ribityl-2′-hydroxyl group of FAD and with the main-chain amide of Glu376, the catalytic base, and these hydrogen bonds cooperatively play a critical role in lowering the pK_a of the substrate α-proton, thereby activating the substrate for deprotonation by the catalytic base. An identical hydrogen-bonding network is found at the thioester carbonyl oxygen of 3-thiaoctanoyl-CoA in a complex with MCAD (*18*). This MCAD-3-thiaoctanoyl-CoA complex has been regarded as a transition-state analog for the reductive half-reaction of MCAD (*18*, *19*). Although the carboxyl group of the fatty acid bound may differ from the thioester moiety of acyl-CoA in its reactivity and structure, the similarity of the hydrogen-bonding network (Figs. 3 and 5) to that of MCAD and the proximity of the Glu421 carboxylate to the fatty acid α-carbon (Figs. 4 and 5) strongly suggest that ACO-II and MCAD share identical machinery for substrate activation/recognition in their reductive half-reactions (Scheme 2). Another point of fundamental importance with respect to catalysis is that the active site does not close upon substrate/product-binding. This implies that the active-site crevice surrounding the flavin ring maintains its ample space regardless of whether the enzyme is in the uncomplexed resting state or in the acting state engaged in the catalytic event with a substrate or product or the intermediate bound therein. Hence, the approach of molecular oxygen to reduced flavin in the oxidative half-reaction is without significant impediment and the oxidative half-reaction with oxygen is structurally favored.

Identification of the Bound Ligand and the Mechanism of Formation—The structure of ACO-II cocrystallized with dodecanoyl-CoA has revealed the presence of a fatty acid species bound within the active-site crevice, as described above. During the cocrystallization experiments and treatments thereafter, we found out that once cocrystallization

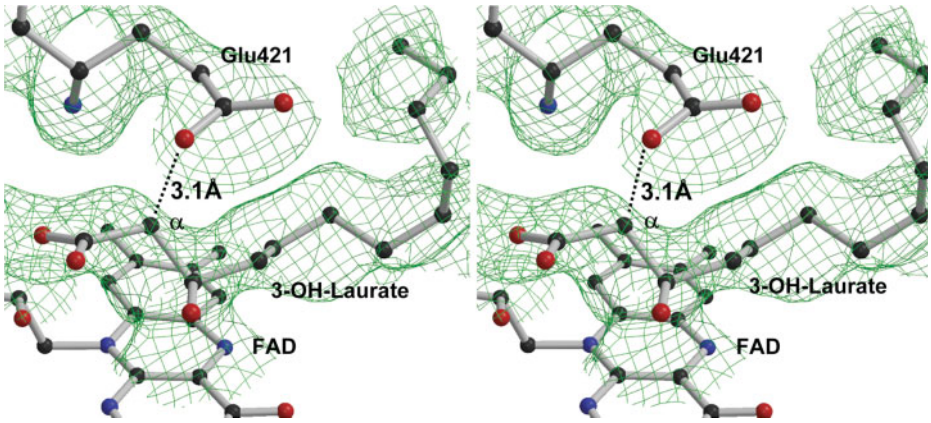

Fig. 4. **Stereo drawing of the 2*Fo*–*Fc* electron density map for bound 3-hydroxydodecanoate and Glu421 contoured at 0.5 σ.**

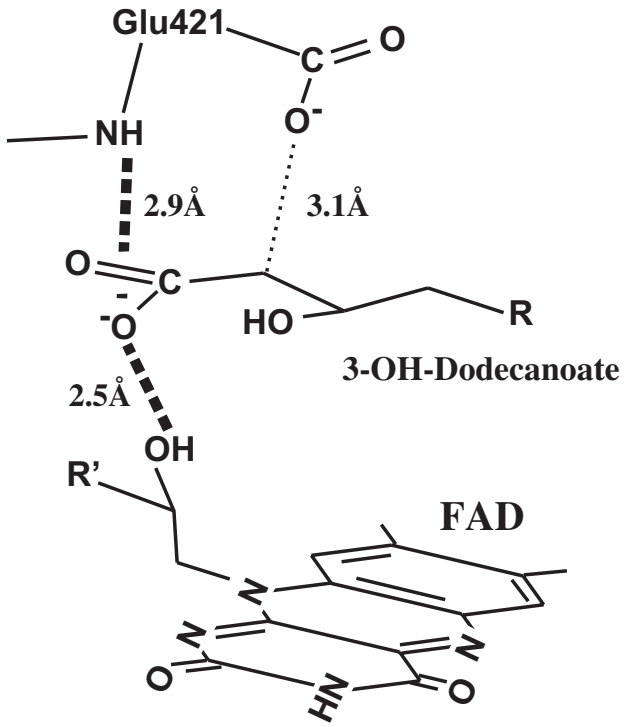

Fig. 5. **Hydrogen-bonding network (thick dashed lines) at the carboxyl oxygen of fatty acid.** The dotted line shows the interatomic distance of 3.5 Å between the α-carbon of the bound fatty acid and the carboxyl oxygen of Glu421 in uncomplexed ACO-II (see text for details).

was completed further added dodecanoyl-CoA did not exchange with the bound fatty acid, *i.e.*, the crystals showed electron density only for the fatty acid, *i.e.*, none for the CoA moiety (results not shown). Furthermore, the addition of dodecanoate to crystalline unliganded ACO-II did not result in the formation of a crystalline ACO-II-fatty acid complex. These observations and the reaction mechanism described below support the idea that the fatty acid species bound in the active site of the crystalline ACO-II are formed during catalysis and in equilibrium with those in the mother liquor. However, the precise structure of the bound ligand remained ambiguous at this point, since the electron-density map was not sufficient to distinguish whether the bound fatty acid is saturated or unsaturated, or includes other minor modifications. So we extracted the fatty acid species from hanging drops containing crystals grown in the presence of excess dodecanoyl-CoA (see "MATERIALS AND METHODS"). The extracts were then subjected to mass spectral analyses. The results shown in Fig. 6 clearly indicate only two mass spectral species at m/z 197.1 and 215.1. The former corresponds to dodecenoate, *i.e.*, mono-unsaturated C12 fatty acid (C12:1), while the latter, the predominant species, can be assigned as hydroxylated dodecanoate. Furthermore, the peak at m/z 199.1 corresponding to dodecanoate (C12:0), the saturated fatty acid, is buried, if present, within the second isotope peak of C12:1. This indicates that non-enzymatic hydrolysis of dodecanoyl-CoA or its inefficient hydrolysis catalyzed at a site other than the active site of crystalline ACO-II hardly occurred, further suggesting mechanism-based formation of the fatty acids within the active site. Dehydration by electric energy may convert hydroxydodecanoate to dodecenoate (C12:1) to a lower extent, which somewhat decreases the peak height ratio of hydroxylated to monoene acids.

So the peak at m/z 197.1 in Fig. 6 includes a very minor contribution from mass spectrometry-driven dehydration of hydroxydodecanoate. The appearance of the peak at m/z 215.1 corresponding to hydroxylated dodecanoate in addition to that for dodecenoate was unexpected at the first sight. However, it can be rationalized on the basis of the active-site structure as well as of the substrate-activating machinery. The presence of two fatty acid species, dodecenoate and hydroxydodecanoate, bound within the active-site crevice can be rationalized by dehydrogenation of dodecanoyl-CoA, as the result of normal catalysis, accompanied by the reaction of water with the dehydrogenated product, dodecenoyl-CoA (Scheme 2). During the cocrystallization of ACO-II in the presence of dodecanoyl-CoA, the enzyme in solution turns over, which produces *trans*-2-dodecenoyl-CoA. But once crystals start to form, dodecanoyl-CoA bound to the active site in a favorable orientation for catalysis undergoes rapid dehydrogenation, which converts the substrate to *trans*-2-dodecenoyl-CoA. However, the product-release from the crystalline enzyme is not as fast as in solution, and the product is held for some time within the active site, the hydrogen-bonding

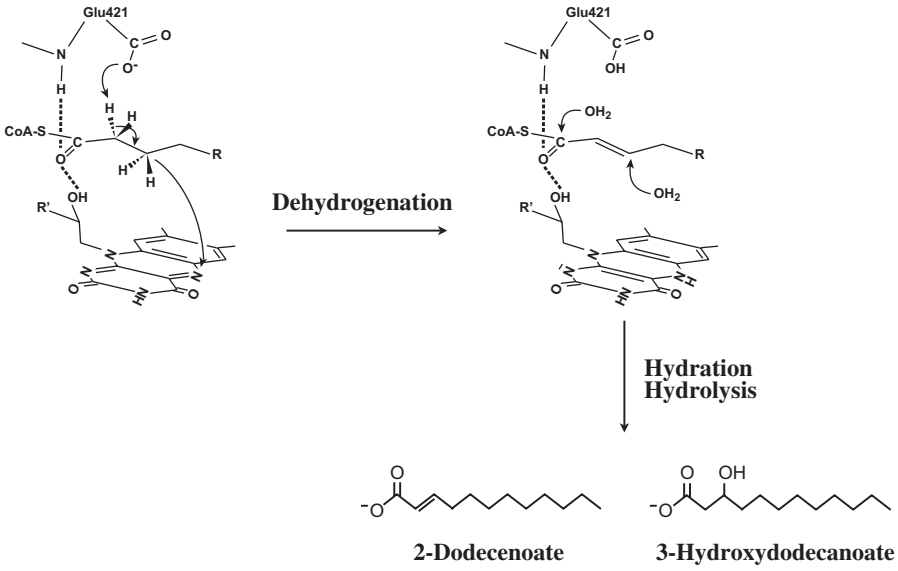

Scheme 2. **The mechanism underlying the reaction of dodecanoyl-CoA during crystal growth and within crystals.**

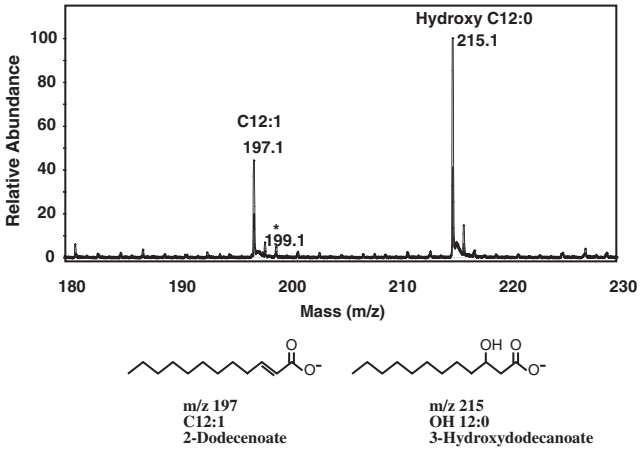

Fig. 6. **Mass spectrogram of the fatty acid species extracted from the crystal preparation of ACO-II in the presence of substrate dodecanoyl-CoA**.

network between thioester carbonyl oxygen and the ribityl-2′-hydroxyl as well as the back-bone amide of Glu421 being retained. This hydrogen-bonding network in turn activates the carbonyl carbon and/or the C(3)-methine carbon of bound dodecenoyl-CoA. As the active-site crevice remains ample during catalysis, water can gain free access to either the carbonyl carbon or C(3)-methine carbon of dodecenoyl-CoA in a Michael-addition type reaction. If water initially attacks the activated carbonyl carbon, thioester is hydrolyzed, which produces dodecenoate, which remains attached to the hydrophobic environment. On the other hand, if water first attacks the C(3)-methine carbon followed by the carbonyl carbon, 3-hydroxydodecanoate forms as the result of Michael addition of water and stays in the hydrophobic pocket. *trans*-2-Dodecenoyl-CoA, which has accumulated during turnover in solution before ACO-II crystallizes, may also penetrate into the active site and will have the same fate as that of the product formed *in situ*, 2-dodecenoate and 3-hydroxydodecanoate eventually being generated. We think that this scenario is a crystallographic artifact primarily due to slow product-release in the crystalline state. Under physiological conditions, however, product-release in solution is much faster and the enzyme turns over preferentially before water attacks the bound product. It should be strongly emphasized, though, that the proposed mechanism for the crystallographic artifact shown in Scheme 2 reflects the inherent modus operandi of ACO-II; the ample active site that allows access of oxygen also allows access of water molecules, and the hydrogen-bonding network at the thioester carbonyl of the substrate activates the substrate for dehydrogenation, but it also activates the product for nucleophilic attack of water in the crystalline state of ACO-II.

We have solved the first structure of ACO in a complex form with a ligand. Although the bound ligand only represents the fatty acid moiety of the substrate or product, the structure has suggested a fundamental mechanism for substrate recognition and activation. Whether or not the conformation and the orientation of the fatty acid bound to the active site accurately reflect the substrate/product-binding mode will be revealed by subsequent study. To answer this question as well as to better understand the substrate activation and the catalytic event at the atomic level, we are attempting to form crystalline ACO in a complex with substrate analogs with a CoA moiety that is not easily hydrolyzed when bound to the active site.

The coordinates for ACO-II in a complex with 3-hydroxydodecanoate have been deposited in the RSCB Protein Data Bank under entry number 2DDH.

This work is supported in part by the National Project on Protein Structural and Functional Analyses.

REFERENCES

1. Ghisla, S. (2004) β-Oxidation of fatty acids. A century of discovery. *Eur. J. Biochem.* **271**, 459–461

2. Matsubara, Y., Indo, Y., Naito, E., Ozasa, H., Glassberg, R., Vockley, J., Ikeda, Y., Kraus, J., and Tanaka, K. (1989) Molecular cloning and nucleotide sequence of cDNAs encoding the precursors of rat long chain acyl-coenzyme A, short chain acyl-coenzyme A, and isovaleryl-coenzyme A dehydrogenases. Sequence homology of four enzymes of the acyl-CoA dehydrogenase family. *J. Biol. Chem*. **264**, 16321–16331
3. Kim, J.-J.P. and Miura, R. (2004) Acyl-CoA dehydrogenases and acyl-CoA oxidases. Structural basis for mechanistic similarities and differences. *Eur. J. Biochem*. **271**, 483–493
4. Setoyama, C., Tamaoki, H., Nishina, Y., Shiga, K., and Miura, R. (1995) Functional expression of two forms of rat acyl-CoA oxidase and their substrate specificities. *Biochem. Biophys. Res. Commun*. **217**, 482–487
5. Nakajima, Y., Miyahara, I., Hirotsu, K., Nishina, Y., Shiga, K., Setoyama, C., Tamaoki, H., and Miura, R. (2002) Three-dimensional structure of the flavoenzyme acyl-CoA oxidase-II from rat liver, the peroxisomal counterpart of mitochondrial acyl-CoA dehydrogenase. *J. Biochem*. **131**, 365–374
6. Pedersen, L. and Henriksen, A. (2005) Acyl-CoA oxidase 1 from *Arabidopsis thaliana*. Structure of a key enzyme in plant lipid metabolism. *J. Mol. Biol*. 345, 487–500
7. Ghisla, S. and Thorpe, C. (2004) Acyl-CoA dehydrogenases. A mechanistic overview. *Eur. J. Biochem.* **271**, 494–508
8. Mizutani, H., Miyahara, I., Hirotsu, K., Nishina, Y., Shiga, K., Setoyama, C., and Miura, R. (2000) Three-dimensional structure of the purple intermediate of porcine kidney D-amino acid oxidase. Optimization of the oxidative half-reaction through alignment of the product with reduced flavin. *J. Biochem*. **128**, 73–81
9. Chayen, N.E. (1997) A novel technique to control the rate of vapour diffusion, giving larger protein crystals, *J. Appl. Cryst.* **30**, 198–202
10. Matthews, B.W. (1968) Solvent content of protein crystals. *J. Mol. Biol.* **33**, 491–497.
11. Otwinowski, Z. and Minor, W. (1997) Processing of X-ray diffraction data collected in oscillation mode. In *Methods in Enzymology* (Carter, C.W., Jr. and Sweet, R.M., eds.) Vol. 276 Part A, pp. 307-326, Academic Press, New York
12. Navaza, J. (1994) *AMoRe*: an automated package for molecular replacement. *Acta Cryst*. **A50**, 157–163
13. Jones, T.A., Zou, J.Y., Cowan, S.W., and Kjeldgaard, M. (1991). Improved methods for building protein models in electron density maps and the location of errors in these models. *Acta Cryst*. **A47**, 110–119
14. Brunger, A.T., Adams, P.D, Clore, G.M., DeLano, W.L., Gros, P., Grosse-Kunstleve, R.W., Jiang, J-S., Kuszewski, J., Nilges, M., Pannu, N.S., Read, R.J., Rice, L.M., Simonson, T., and Warren, G.L. (1998) Crystallography & NMR system: A new software suite for macromolecular structure determination. *Acta Cryst*. **D54**, 905–921
15. Laskowski, R. A., MacArthur, M.W., Moss, D.S., and Thornton, J.M. (1993) *PROCHECK*: a program to check the stereochemical quality of protein structures. *J. Appl. Cryst*. **26**, 283–291
16. Dole, V.P. and Meinertz, H. (1960) Microdetermination of long-chain fatty acids in plasma and tissues. *J. Biol. Chem.* **235**, 2595–2599
17. Kim, J.-J.P., Wang, M., and Paschke, R. (1993) Crystal structures of medium-chain acyl-CoA dehydrogenase from pig liver mitochondria with and without substrate. *Proc. Natl. Acad. Sci. USA* **90**, 7523–7527
18. Satoh, A., Nakajima, Y., Miyahara, I., Hirotsu, K., Tanaka, T., Nishina, Y., Shiga, K., Tamaoki, H., Setoyama, C., and Miura, R. (2003) Structure of the transition state analog of medium-chain acyl-CoA dehydrogenase. Crystallographic and molecular orbital studies on the charge-transfer complex of medium-chain acyl-CoA dehydrogenase with 3-thiaoctanoyl-CoA. *J. Biochem*. **143**, 297–304
19. Lau, S.M., Brantley, R.K., and Thorpe, C. (1988) The reductive half-reaction in acyl-CoA dehydrogenase from pig kidney: studies with thiaoctanoyl-CoA and oxaoctanoyl-CoA analogues. *Biochemistry* **27**, 5089–5095